

Photoluminescence in wide band gap corundum $\text{Mg}_4\text{Ta}_2\text{O}_9$ single crystals*

Liang Li(李亮), Yu-Lu Zheng(郑雨露), Yu-Xin Hu(胡雨馨), Fang-Fei Li(李芳菲),
Qiang Zhou(周强)[†], and Tian Cui(崔田)

State Key Laboratory of Superhard Materials, College of Physics, Jilin University, Changchun 130000, China

(Received 14 February 2020; revised manuscript received 9 April 2020; accepted manuscript online 17 April 2020)

As is well known, the basic intrinsic properties of materials can be significant for their practical applications. In this work, the room-temperature absorption, transmittance, reflectance spectra, and relative photoelectricities parameters of the $\text{Mg}_4\text{Ta}_2\text{O}_9$ crystals are demonstrated. Meanwhile, the polarized Raman spectra of $\text{Mg}_4\text{Ta}_2\text{O}_9$ crystals are also described. The room-temperature photoluminescence (PL) and the temperature-dependent PL for $\text{Mg}_4\text{Ta}_2\text{O}_9$ crystals are obtained. Significantly, we observe a phonon-participated PL process in $\text{Mg}_4\text{Ta}_2\text{O}_9$.

Keywords: corundum, band gap energy, polarized Raman, photoelectric, ultraviolet emission

PACS: 33.20.Fb, 61.05.Cp, 07.55.Jg

DOI: 10.1088/1674-1056/ab8a3d

1. Introduction

The wide band gap semiconductor materials have received more and more attention because they render the light-emitting devices possible.^[1–4] As a wide band gap semiconductor, the corundum $\text{Mg}_4\text{Ta}_2\text{O}_9$ with a high dielectric performance attracts much more attention due to its possible applications in serving as luminescent^[5–7] and microwave dielectric resonator materials.^[8] However, the $\text{Mg}_4\text{Ta}_2\text{O}_9$ that has been obtained so far is just in the form of powders^[9–11] or thin films.^[8,12,13]

The optical properties of $\text{Mg}_4\text{Ta}_2\text{O}_9$ are very important, for they can involve many basic physics problems related to the energy levels and show the possibilities in some optical equipment applications.^[14–17] Furthermore, light emitting devices which are based on semiconductor have been found to have many applications, such as in water purification equipment and surface purification, food preservation devices, and new sorts of communication system.^[1,18] Meanwhile, it is significant to well know the intrinsic properties of materials in their application.^[19,20] However, the boundaries and some twin structures in materials can influence their characters and applications significantly. So, the significance for studying well oriented crystals to overcome these extrinsic effects lies not only in their practical applications, but also in their fundamental research.^[21,22]

Previously, high-quality corundum $\text{Mg}_4\text{Ta}_2\text{O}_9$ single crystals have been achieved by the optical floating zone method.^[23] In this work, we investigate the experimental band gap energy and strong near-infrared (NR) emission from corundum $\text{Mg}_4\text{Ta}_2\text{O}_9$, which may open the door for a large number of potential applications in many fields including laser

diodes, NR light-emitting devices (NRLEDs), *etc.*

Moreover, it is important to investigate the optical phonon behaviors of $\text{Mg}_4\text{Ta}_2\text{O}_9$ for its potential applications in NRLED and laser active media. Furthermore, the response of the material to microwave dielectric can also be achieved from the intrinsic contribution of its polarized phonons. In addition, the nonradioactive decay is mainly dependent on the phonons in the laser crystals, which may be harmful effect in some circumstances. The Raman scattering is a useful approach to studying the optical phonon behavior of the materials.^[22,24,25] So, the polarized Raman spectra are also investigated in the present work. Furthermore, a phonon participating in the PL process is exactly observed from room temperature PL.

2. Experiment procedure

Transparent and colourless corundum $\text{Mg}_4\text{Ta}_2\text{O}_9$ crystals were obtained via the optical floating zone technology, previously. And we have prepared a crystal slice for optical measurements, which was cut and finely polished along the *c* axis direction into 3.0 mm×5.1 mm×0.7 mm in dimension, as shown in the insert of Fig. 1(a). And the structure and orientation of the as-grown crystals were identified previously.^[23]

The absorption and transmission spectra were measured via Shimadzu UV-VIS-3600 spectrophotometer at room-temperature. Both the PL spectra and polarized Raman spectra measurements were performed by the Jobin Yvon High Resolution 800 Raman spectrometer in the backscattering geometry with polarized plate, half wave plate, the 514.5-nm excitation line from the Spectra Physics Stabilize 2017 Ar ion laser and Linkam THS600 Thermal stage.

*Project supported by the National Key Research and Development Program, China (Grant No. 2017YFA0403704), the National Natural Science Foundation of China (Grant Nos. 11304113, 11474127, and 11574112), and the Fundamental Research Funds for the Central Universities, China.

[†]Corresponding author. E-mail: zhouqiang@jlu.edu.cn

3. Results and discussion

Figure 1(a) displays the obtained transmittance spectrum of the $\text{Mg}_4\text{Ta}_2\text{O}_9$ crystal sample. The transmittance for the $\text{Mg}_4\text{Ta}_2\text{O}_9$ crystal wafer reaches up to 75% in the visible and near-infrared region (from 325 nm to 1000 nm). But the transmittance becomes lower suddenly at a lower wavelength (< 325 nm), which is called ultraviolet (UV) region. So, we can achieve a lower cutoff wavelength of $\text{Mg}_4\text{Ta}_2\text{O}_9$, about 325 nm.

Figure 1(b) shows the $\text{Mg}_4\text{Ta}_2\text{O}_9$ crystal wafer absorption spectrum along the c -axis direction. The crystal has a low absorption coefficient (α) (about 1.4 cm^{-1}) in a wavelength range from 1000 nm to 325 nm, a transparent region. As for ultraviolet region (< 325 nm), the crystal has a strong absorption.

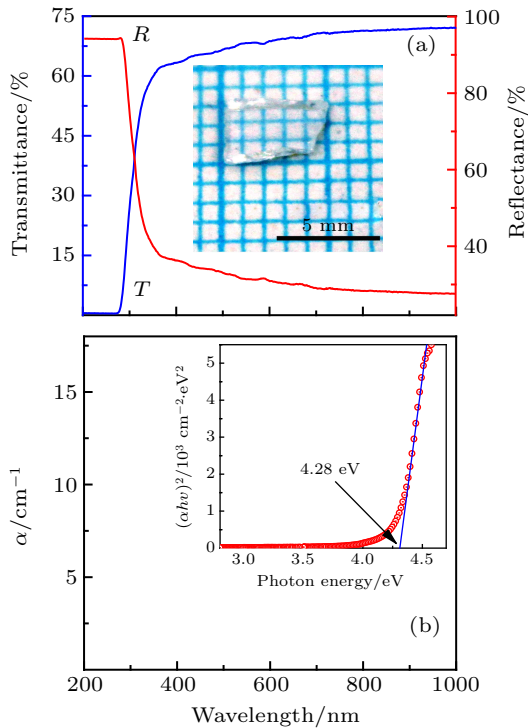


Fig. 1. (a) Room-temperature transmittance and reflectance spectrum, with insert showing $\text{Mg}_4\text{Ta}_2\text{O}_9$ crystal wafer, and (b) absorption spectrum with insert showing variation of $(\alpha hv)^2$ with photon energy ($h\nu$) of as-grown $\text{Mg}_4\text{Ta}_2\text{O}_9$ crystal.

Photon energy $h\nu$ can be related to the absorption coefficient by the following equation

$$\alpha h\nu = (h\nu - E_g)^k, \quad (1)$$

where k takes the value of $1/2$, or 2 , or $3/2$, or 3 to allow direct transition, or indirect transition, or forbidden direct transition, or indirect transition, respectively. For the $\text{Mg}_4\text{Ta}_2\text{O}_9$ crystal, the best k is taken to be $1/2$, which demonstrates that $\text{Mg}_4\text{Ta}_2\text{O}_9$ is a direct transition material, and it also accords well with previous theoretical result.^[26] The band gap energy is achieved to be 4.28 eV by extrapolating the linear region of $(\alpha hv)^2$ versus $h\nu$ as shown in Fig. 1(b). Notably, this is

the first time that the band gap energy of $\text{Mg}_4\text{Ta}_2\text{O}_9$ has been demonstrated experimentally.

Within the transparent range of $\text{Mg}_4\text{Ta}_2\text{O}_9$ crystal, T can be described by the reflectance (R) and α from the crystal wafer by^[27]

$$T = \frac{(1 - R)^2 \exp(-\alpha d)}{1 - R^2 \exp(-2\alpha d)}, \quad (2)$$

where $d = 0.7 \text{ mm}$ is the thickness of the crystal wafer. The reflectance spectrum for $\text{Mg}_4\text{Ta}_2\text{O}_9$ crystal wafer is achieved from the transmittance and absorption spectra via Eq. (2) as depicted by the red line in Fig. 1(a). The reflectance spectrum shows a similar tendency to the absorption spectrum, in which the $\text{Mg}_4\text{Ta}_2\text{O}_9$ crystal has a lower reflection in the wavelength range from 1000 nm to 325 nm. Up to the ultraviolet region (< 325 nm), the crystal has a strong reflection.

The relationship among extinction K , refractive index n and R is related by the following expression:^[28]

$$K = \frac{\alpha \lambda}{4\pi}, \quad R = \frac{(n - 1)^2 + K^2}{(n + 1)^2 + K^2}, \quad (3)$$

where λ is the wavelength. Spectrum of K and n are obtained from T and α spectrum by calculating Eq. (3), and the results are described in Fig. 2(a). The refractive index of $\text{Mg}_4\text{Ta}_2\text{O}_9$ is high before 400 nm, and after that λ decreases fast.

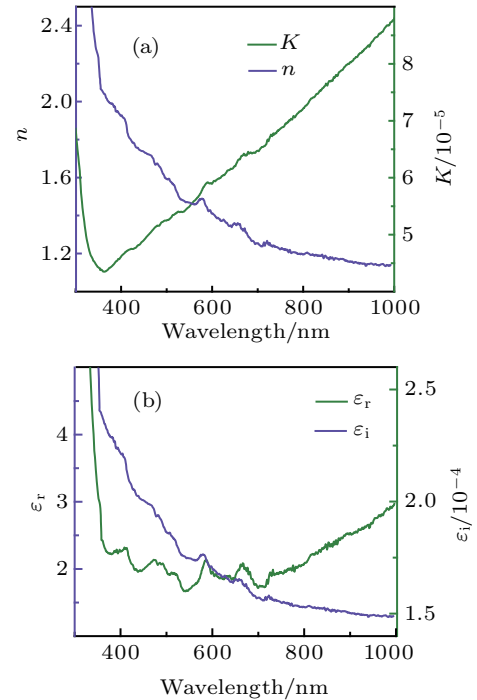


Fig. 2. (a) Refractive index and extinction coefficient versus wavelength, and (b) dielectric constant and dielectric loss factor versus wavelength of $\text{Mg}_4\text{Ta}_2\text{O}_9$.

Then we introduce the following equation:^[28]

$$\epsilon_i = 2nK, \quad \epsilon_r = n^2 - K^2, \quad (4)$$

where ϵ_i is the imaginary and ϵ_r is the real parts of complex dielectric ϵ . From Fig. 2(a) and Eq. (4), the ϵ_r and ϵ_i of $\text{Mg}_4\text{Ta}_2\text{O}_9$ are obtained.

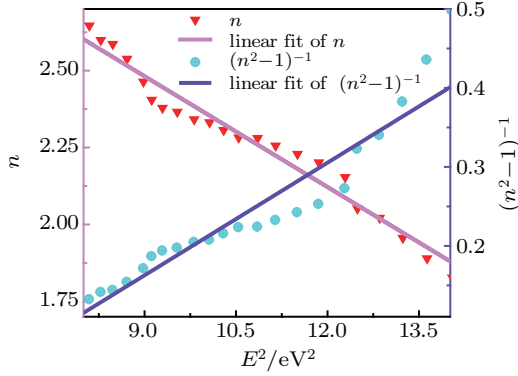


Fig. 3. Plot of n and $(n^2 - 1)^{-1}$ versus E^2 of $\text{Mg}_4\text{Ta}_2\text{O}_9$.

Urbach tail defined as the energy under the band gap ($E < E_g$). The n versus energy (E) expressed as the Cauchy–Sellmeier function is related by the following expression:^[28]

$$n(E) = n_0 + a_1 E^2, \quad (5)$$

in which n_0 and a_1 are constants. Linearly fitting n versus E^2 in the range between 8 eV² and 14 eV² is shown in Fig. 3. The n_0 and a_1 are 0.8 and 0.04, respectively.

The area below the band-to-band absorption edge, due to their correspondence to the fundamental electronic excitation properties, the refractive index dispersion is very important for us to learn the dielectric characteristics of materials. By using the single-effective oscillator model, many samples in the solid and liquid forms were validated.^[29,30] Using Krammers–Kronig relation, the ϵ_r can be described as^[28]

$$\epsilon_r = 1 + \frac{F}{(E_0^2 + E^2)}, \quad (6)$$

in which E is the energy of photons, F is the single oscillator energy, E_0 depends on the oscillator transition frequency and the strength of electric dipole. And the parameters can be specially combined as follows:^[29,30]

$$E_d = F/E_0, \quad (7)$$

where E_d is the dispersion energy. By ignoring K value between 2.2 eV and 3.5 eV, equations (5) and (6) are combined into the following equation:^[30]

$$\epsilon_r(E) = n^2(E) = 1 + \frac{E_d E_0}{(E_0^2 - E^2)}. \quad (8)$$

According to the α and T spectrum in the energy range, the K and n of $\text{Mg}_4\text{Ta}_2\text{O}_9$ crystal can be easily obtained. By linearly fitting $(n^2 - 1)^{-1}$ versus E^2 in Fig. 3, we can obtain the E_d and E_0 to be 2.47 eV and 3.45 eV, respectively. On the other hand, we achieve that the static refractive index $n(0) = 0.8$ and static dielectric constant $\epsilon_s = n^2(0) = 2.40$.

In corundum $\text{Mg}_4\text{Ta}_2\text{O}_9$, the cations are arrayed along the c axis. The MgO_6 octahedrons connect to the other MgO_6 octahedrons by sharing edges and faces. Meanwhile, the TaO_6

octahedrons connect to the other TaO_6 octahedrons via sharing faces and connect to the MgO_6 octahedrons via sharing edges as shown in the insert of Fig. 4.^[31,32] The band structure of $\text{Mg}_4\text{Ta}_2\text{O}_9$ can be observed through the relations between oxygen and cations in the octahedron. The conduction band Ta^{5+} is 5d orbitals. While the valence band of $\text{Mg}_4\text{Ta}_2\text{O}_9$ is presumed to be O^{2-} 2p orbitals.^[32]

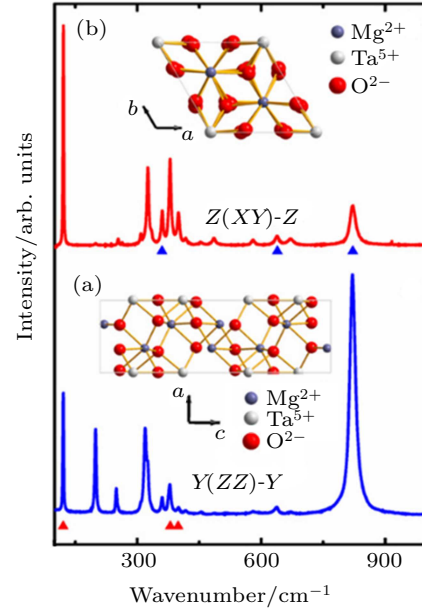


Fig. 4. Polarized Raman spectrum in (a) $Y(ZZ)-Y$ and (b) $Z(XY)-Z$ geometry, with inserts showing view direction along b and c axes of $\text{Mg}_4\text{Ta}_2\text{O}_9$ single crystal, respectively.

The orientation and conformation of single crystal can activate special vibration modes by changing the proper polarization direction of the incident and scattered light. So, the polarized Raman spectrum of single crystal is utilized for assigning the vibrations, which cannot be proved by unpolarized Raman spectrum with the same wavenumber. On the other hand, the space group of $\text{Mg}_4\text{Ta}_2\text{O}_9$ is $P-3c1(165)$ and the point group is $D_{3d}(-3m)$. There are $7A_{1g}$ and $15E_g$ that are both Raman active (R) according to the group theory analysis. Meanwhile, Raman tensors can be expressed as follows:

$$A_{1g} = \begin{pmatrix} a & 0 & 0 \\ 0 & a & 0 \\ 0 & 0 & b \end{pmatrix}, \quad E_{g,1} = \begin{pmatrix} c & 0 & 0 \\ 0 & -c & d \\ 0 & d & 0 \end{pmatrix},$$

$$E_{g,2} = \begin{pmatrix} 0 & -c & -d \\ -c & 0 & 0 \\ -d & 0 & 0 \end{pmatrix}.$$

And based on polarization selection rule and the Raman tensor, the A_{1g} and E_g can be obtained in $Y(ZZ)-Y$ and $Z(XY)-Z$, respectively, under back scattering geometry. In this study, the angle of XY is 120° , so a half-wave plate is used. The polarized Raman spectrum of $\text{Mg}_4\text{Ta}_2\text{O}_9$ crystal is obtained as shown in Fig. 4. All the Raman peaks in the spectra can be assigned to in the whole wavenumber range.^[23,33] In the $Y(ZZ)-Y$ configuration (Fig. 4(a)), the spectrum is dominated by A_{1g}

model at 820 cm^{-1} and all other six A_{1g} models at 200 cm^{-1} , 250 cm^{-1} , 320 cm^{-1} , 361 cm^{-1} , 454 cm^{-1} , and 639 cm^{-1} are achieved properly. While in the $Z(XY)-Z$, all 13 E_g bands (128 cm^{-1} , 254 cm^{-1} , 263 cm^{-1} , 309 cm^{-1} , 326 cm^{-1} , 335 cm^{-1} , 379 cm^{-1} , 400 cm^{-1} , 418 cm^{-1} , 486 cm^{-1} , 580 cm^{-1} , and 672 cm^{-1}) are observed in this range. And the strongest mode in this configuration is E_g model at 128 cm^{-1} as shown in Fig. 4(b). Meanwhile, there are some other bonds in special polarized configuration marked by related symbols (A_{1g} and E_g models are marked in blue and red, respectively). The peaks which do not belong to our polarized configuration but appear should be attributed to the complex structure, little disorientation of the $\text{Mg}_4\text{Ta}_2\text{O}_9$ crystals or the dazzle effect of the lens. In general, these phenomena reflect the Raman selection rules. The occurrence of the highest energy and second strongest peak at 820 cm^{-1} are due to the symmetry stretching models of terminal Ta–O chain between the face-shared two TaO_6 octahedra. The peak located at 580 cm^{-1} with a lower energy can be attributed to the stretching mode of the bridged Ta–O bond. We can identify the peaks at 672.7 cm^{-1} and 637.2 cm^{-1} as two chain Ta–O bonds, and the close bonding energy and length lead the chain bonds to appear, so their wavenumbers are close to each other. The puzzling peaks from 300 cm^{-1} to 500 cm^{-1} come from the vibrations of MgO_6 octahedra. Meanwhile, the mode at 128 cm^{-1} , having the strongest intensity and the lowest energy, can be assigned to an additional mode that forms the Ta–Ta stretching bonds between the two TaO_6 octahedra connected by face-shared oxygens^[34] as shown in Table 1.

Table 1. Vibrational modes of $\text{Mg}_4\text{Ta}_2\text{O}_9$.

Raman mode	Assignment	f/cm^{-1}
E_g	Ta–Ta stretching	128
A_{1g}	bending vibration in the O–Ta–O	200
		250
E_g	bending vibration in the O–Ta–O	254
		263
A_{1g}	MgO_6 octahedrons	320
		361
		454
		309
		326
		335
E_g	MgO_6 octahedrons	361
		379
		400
		418
		486
E_g	bridged Ta–O stretching	580
A_{1g}	two Ta–O chain stretchings	639
E_g	Ta–O stretching	672.2
		672.7
A_{1g}	symmetric Ta–O stretching	820

Figure 5(a) shows the room-temperature PL spectrum of $\text{Mg}_4\text{Ta}_2\text{O}_9$. The PL peak can be well fitted to two emission peaks centered at 821.19 nm (1.51 eV) and 770.19 nm (1.61 eV) by using Gaussian fitting. Significantly, the PL emission centers at 1.51 eV – 1.61 eV and instead of the obtained band gap ($\sim 4.28\text{ eV}$) from $\text{Mg}_4\text{Ta}_2\text{O}_9$ excited by using laser line of 514 nm at room temperature, which cannot be attributed to the normal band-to-band transitions. The mechanism of $\text{Mg}_4\text{Ta}_2\text{O}_9$ luminescence can be compared to that of the solid with niobate–oxygen octahedron due to their identical outer electronic configuration. In the $\text{PbMg}_{1/3}\text{Nb}_{2/3}\text{O}_3$ – $\text{PbIn}_{1/2}\text{Nb}_{1/2}\text{O}_3$ systems, the special luminescence tends to relate to the origin of PL bands with the Nb–O system without influence of Mg and Pb. The two PL peaks at 1.61 eV and 1.51 eV of $\text{Mg}_4\text{Ta}_2\text{O}_9$ are consistent with the A (with a weaker intensity and higher energy) and B (with a stronger intensity and lower energy), which are mainly determined by the defect and regular Ta–O respectively. To understand the observed phenomenon, we need to consider the non-radiative transition of exciton in the schematic band diagram as shown in Fig. 5(b). The photo-excitation allows electrons in the oxygen state in the valence band (V_o) to transit to the conduction band (CB), leaving holes in the V_o , and then the excited electrons in the CB relax to intrinsic Ta_i after a non-radiative (NR) transition process. Eventually, the relaxed electrons recombine with holes, and thus cause the PL emission. There will be two possible types in this case: one is the B peak and the other is the A peak which is caused by defect states. Moreover, the energy difference between A and B excitons is 0.10 eV , corresponding to the relative vibration energy 820 cm^{-1} that corresponds to the strongest peak in Raman spectrum and can be assigned to the symmetry stretching model of terminal Ta–O chain between the face-shared two TaO_6 octahedrons. It well illustrates that the phonons participate in the recombination process of excitons. Therefore, the defect emission A is from the electrons recombining with holes directly, while the B originates from the emission and vibration and the relaxing of photon and phonon.

The temperature-dependent PL spectra of $\text{Mg}_4\text{Ta}_2\text{O}_9$ crystal in a range from 85 K to 805 K are present at Fig. 5(c). As the temperature increases, the intensity of PL presents a decrease tendency and quenches at 605 K as shown in Fig. 5. One of the main reasons for reducing the intensity can be attributed to the thermodynamic movement of molecules. It is possible to convert the excitation energy into vibrational energy of the ground state, and when the excited molecule receives additional thermal energy, the rapid vibration and relaxation will lead the vibration energy to lose. And the two peaks of temperature-dependent PL emission can also be fitted by Gaussian. The temperature-dependent values of the two

peak centers in a temperature range from 85 K to 605 K are shown in Fig. 5(d). As the temperature increases, both of the two centers show blueshifts linearly and we fit the two data linearly. The shift speed of defect A bond (1.2×10^{-4} eV/K) is slightly faster than that of the B bond (0.9×10^{-4} eV/K). The

blueshifts can be attributed to the shrinkage of Ta_i-CB and V_o-VB, and resulting in the fact that the broadening of recombination energy between Ta_i and V_o. The lower blueshift speed of regular B bond should be due to the phonons at 820 cm⁻¹ having a lower thermal response.^[23]

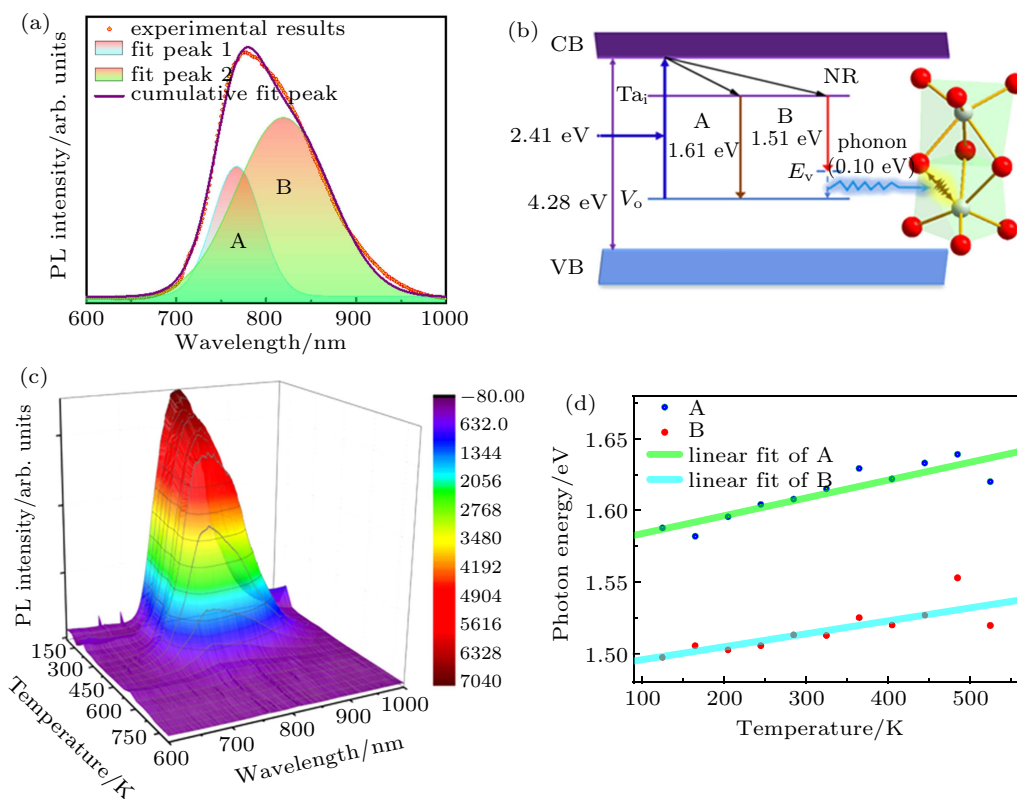


Fig. 5. (a) PL spectrum of Mg₄Ta₂O₉ crystal at room temperature, (b) schematic band diagram with phonon excitation, A and B emission process and non-radiative transition, (c) temperature-dependent PL spectra of Mg₄Ta₂O₉ crystal, and (d) two temperature-dependent fitted peak centers in a range from 85 K to 605 K.

4. Conclusions

The lower cutoff wavelength of the Mg₄Ta₂O₉ is 325 nm obtained from the room-temperature transmittance spectrum. The Mg₄Ta₂O₉ is a direct transition material and band gap energy is determined to be 4.28 eV. The reflectance spectrum of Mg₄Ta₂O₉ is also presented. Useful photoelectricity parameters of Mg₄Ta₂O₉ are obtained. Additionally, the Raman selection rules for the Mg₄Ta₂O₉ crystal are estimated and the vibrations of Raman bonds are assigned. In particular, the PL spectra centered at 1.51 eV and 1.61 eV are observed to be dependent on the regular Ta-O system and defective Ta-O system respectively. The phonons at 820 cm⁻¹ (0.10 eV) are found to participate in the PL process. Furthermore, the temperature-dependent PL spectra are also discussed.

References

- [1] Huang M H, Mao S, Feick H, Yan H, Wu Y, Kind H, Weber E, Russo R and Yang P 2001 *Science* **292** 1897
- [2] Koizumi S, Watanabe K, Hasegawa M and Kanda H 2001 *Science* **292** 1899
- [3] Xiao J, Liu P, Wang C X and Yang G W 2017 *Prog. Mater. Sci.* **87** 140
- [4] Jiang Y, Xia H, Zhang J, Yang S, Jiang H and Chen B 2015 *J. Mater. Sci. Tech.* **31** 1232
- [5] Blasse G and Bril A 1971 *J. Solid State Chem.* **3** 69
- [6] Stevels A and Vink A 1974 *J. Lumin.* **8** 443
- [7] Macke A J H 1976 *J. Solid State Chem.* **19** 221
- [8] Sun D C, Senz S and Hesse D 2004 *J. Eur. Ceram. Soc.* **24** 2453
- [9] Navale S C and Ravi V 2005 *Mater. Sci. Eng.: B* **119** 189
- [10] Gaikwad A B, Navale S C, Samuel V, Murugan A V and Ravi V 2006 *Mater. Res. Bul.* **41** 347
- [11] Wu H T, Yang C H, Wu W B and Yue Y L 2012 *Surf. Rev. Lett.* **19** 1250024
- [12] Huang C and Chen J 2009 *J. Cryst. Growth* **311** 627
- [13] Sun D, Senz S and Hesse D 2006 *J. Eur. Ceram. Soc.* **26** 3181
- [14] Coldea R, Tennant D, Wheeler E, Wawrzynska E, Prabhakaran D, Telling M, Habicht K, Smeibidl P and Kiefer K 2010 *Science* **327** 177
- [15] Yang Z, Chang Y and Wei L 2007 *Appl. Phys. Lett.* **90** 042911
- [16] Leite D M G and Silva J H D 2008 *J. Phys.: Condens. Matter* **20** 055001
- [17] Zhuo S Y, Liu X C, Huang W, Kong H K, Xin J and Shi E W 2019 *Chin. Phys. B* **28** 017101
- [18] Noh Y W, Jin I S, Park S H and Jung J W 2019 *J. Mater. Sci. Technol.*
- [19] Yu X, Cui H, Zhu M, Xia Z and Sai Q 2019 *Chin. Phys. B* **28** 077801
- [20] Xue Y, Zheng L, Jiang D, Sai Q, Su L and Xu J 2019 *Chin. Phys. B* **28** 037802
- [21] Yao T S, Tang C Y, Yang M, Zhu K J, Yan D Y, Yi C J, Feng Z L, Lei H C, Li C H and Wang L 2019 *Chin. Phys. Lett.* **36** 068101
- [22] Li Y W, Wang X, Li G W, Wu Y, Pan Y Z, Xu Y B, Chen J and Lei W 2020 *Chin. Phys. Lett.* **37** 018101

- [23] Li L, Liu W, Han B, Jin X, Li F, Wang W, Zhou Q, Xu D and Cui T 2015 *RSC Adv.* **5** 66988
- [24] Niu X, Zhang H, Pei Z, Shi N, Sun C and Gong J 2019 *J. Mater. Sci. Technol.* **35** 88
- [25] Chen P, Zeng S, Zhao Y, Kang S, Zhang T and Song S 2020 *J. Mater. Sci. Technol.* **41** 88
- [26] Mei Q J, Li C Y, Guo J D, Huang S X, Zhang X H and Wu H T 2013 *Ceram. Int.* **39** 9145
- [27] Li L, Fan Y, Wang D, Feng G and Xu D 2011 *Cryst. Res. Technol.* **46** 475
- [28] Xu D, Gu Y, Li L, Shen H, Yang H, Zhou Q, Shi Z, Yuan H and Cui T 2014 *J. Phys. Chem. Solids* **75** 1361
- [29] Wemple S H and DiDomenico M 1969 *Phys. Rev. Lett.* **23** 1156
- [30] Wemple S H and DiDomenico M 1971 *Phys. Rev. B* **3** 1338
- [31] Kan A, Ogawa H, Yokoi A and Nakamura Y 2007 *J. Eur. Ceram. Soc.* **27** 2977
- [32] Ogawa H, Kan A, Ishihara S and Higashida Y 2003 *J. Eur. Ceram. Soc.* **23** 2485
- [33] Gui D Y, Wang C H, Zhu W and Meng C 2018 *J. Alloys Compd.* **730** 434
- [34] Li L, Duan D, Zhou Q, Xu D, Cui T, Liu B, Shi Z and Yuan H 2015 *J. Alloys Compd.* **619** 240